Autocorrelation Function of Smooth Surfaces from Integrated Wavelet Transforms

Aristide C. Dogariu and Glenn D. Boreman
CREOL, University of Central Florida
12424 Research Pkwy, Suite 400, Orlando, FL 31816

Abstract

The surface autocorrelation function can be retrieved from the values of the far-field integrated irradiance. The inversion procedure is discussed in the frame of a theory of integrated wavelet transformation. For different types of autocorrelation functions, the capabilities and limitations of the inversion procedure are studied. The influence of experimental noise and the specific choice of the analyzing wavelet are also investigated.

Keywords: surface scattering, roughness, inverse problem, wavelet transform

I. Introduction

The microtopography of real surfaces affects the wave scattering behavior and the wave-surface interaction has been a common tool for characterization of rough surfaces. Despite the intensive research in the area of surface scattering, the general scattering problem has yet to be solved. However, regimes of surface roughness measurable with light scattering have been established[1] and various measuring techniques have been proposed. Due to their noncontact style of measurement, speed and adjustment capabilities, the optical methods for roughness measurement are most suitable for on-line evaluation or inspection of surface roughness, on the control of polishing process in automatic procedures.

The topography of a rough surface can be described by the statistical distribution of heights $z(\mathbf{x})$ measured from a reference plane as a function of lateral position $\mathbf{x}$. It has been shown that a Gaussian statistics of heights provide an accurate description of most real surfaces.[2] The classical description of surface roughness uses two parameters: the root-mean-square deviation of the height of the surface profile $\sigma = \sqrt{< z(\mathbf{x})^2 >}$, provided that $< z(\mathbf{x}) >= 0$, and the

autocorrelation function (ACF) $C(\mathbf{x}) = \sigma^2 < z(\mathbf{x}+\mathbf{x}')z(\mathbf{x}') >$ characterizing the distribution of roughness over the surface. Note that σ refers to the description of *vertical* roughness while $C(\mathbf{x})$ takes into account the *horizontal* length scales involved in the surface profile. For a smooth surface $\sigma << L$ and $\sigma << \lambda$ where L is the correlation length on the surface profile and λ is the wavelength of the incident radiation. Most surfaces in the industrial environment can be categorized as smooth or moderately rough surfaces.

II. Scattering from smooth surfaces

In the smooth surface limit, the specular component of the intensity scattered in the far-field is proportional to the variance of the surface fluctuations σ^2 and this offers a direct and simple possibility to measure and monitor the r.m.s roughness σ. The diffuse component of the far-field intensity is well approximated by a Fourier transform of the ACF multiplied by the surface variance $I_{diff}(\mathbf{k}) \sim \sigma^2 C(\mathbf{x})$.

Monitoring the r.m.s roughness σ offers only limited information about the *vertical* roughness and, in order to complete the surface description, one is required to make far-field angular-resolved intensity measurements. On this basis, two different approaches provide the surface description. First, a direct and easy way is to assume a certain ACF and to compare directly the angle-resolved scattering data with roughness-model-dependent theories in order to find the model parameters. Second, one can solve the inverse problem and describe the surface statistics without any initial assumptions about the ACF. In the case of smooth surfaces practical difficulties are encountered in retrieving ACF. The intensities in the diffuse component are several orders of magnitude weaker than the specular component and, moreover, one needs to record the angular-dependent intensities over as large an angular domain as possible. The wide dynamic range required for the detection system imposes serious experimental limitations such as the normalization of the angular sensitivity. In addition, the speckle noise significantly affects the variation of the intensity for small changes of the scattering angle. This effect must be averaged out by moving the sample or the detector while recording a large number of scattering-data points. Another practical difficulty arises when the investigated surface is not isotropically rough. The attempts to average out the speckle effect should be, in this case, carefully correlated to the directional features of the surface.

The classical procedures for characterization of smooth surfaces are angle-resolved scattering (ARS)[34] and the total integrated scattering (TIS)[5] techniques. In the ARS, the scattered intensity is measured as a function of the scattering angle and the inverse problem is solved from the Fourier transformation of the scattering data or from the least-square fitting of a conventional scalar scattering function to the experimental data. The practical difficulties are the need for normalization of the relative sensitivities in the detection system and the deterioration of the angular resolution when enlarging the detection aperture to smooth out the speckle effect. In the TIS technique, the scattered light is integrated over the hemisphere containing the incident, reflected and scattered beams. This method overcomes the problem of speckle noise. However,

in order to solve the inverse problem, the values of the integrated intensity as a function of wavelength are needed. Meanwhile, TIS cannot offer the possibility to reconstruct ACF in the case of anisotropic surfaces.

An alternative method of using the far-field intensity distribution is to make far-field integrated irradiance measurements in an experiment such as suggested in Fig. 1.

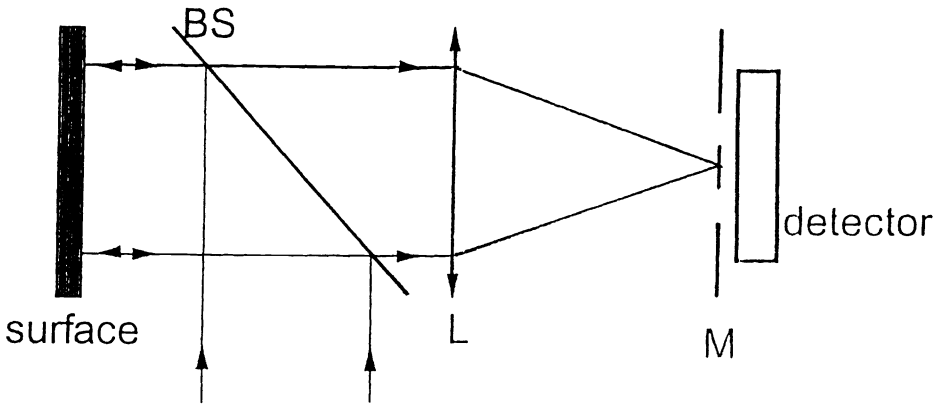

Fig.1 Experimental setup for measuring the far-field integrated irradiance.

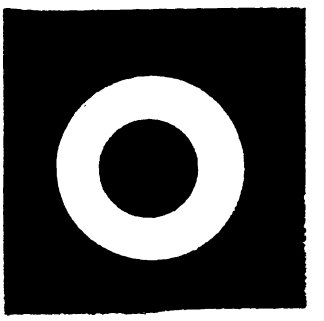

Fig. 2 Annular filter placed in the focal plane of the lens L in Fig.1.

Values of the integrated irradiance are measured as a function of the size of the ring-like filter M in the Fourier plane of the collecting lens L. Note that, due to the large area of the filter M, this kind of measurement enhances the contribution of small intensities at large scattering angles and, meanwhile, completely eliminates the speckle noise. Besides, by using an annular filter, the specular component of the scattered intensity is directly removed. The values of the integrated irradiance as a function of filter magnification have been successfully used in the measurement of surface roughness and the correlation length of surface profiles.[6]

III. Integrated irradiance

Let us consider the light scattering from a rough surface described by an autocorrelation function $C(x)$. The corresponding far-field diffuse intensity is $i(k)$ is proportional to the Fourier transform of $C(x)$ and, therefore, contains all the information about the surface roughness. The far-field irradiance is measured through a filter M described by $G(k,a) = 1$ if $k_1/a \leq k \leq k_2/a$ and $G(k,a) = 0$ for $k < k_1/a$ or $k > k_2/a$, where k_1 and k_2 are constants that determine the shape of the filter and a is a parameter describing the magnification of the filter. In Fig. 2 we present such a ring filter corresponding to a ratio $k_2/k_1 = 5/2$. The integrated irradiance measured through the filter M can be regarded as a function of magnification parameter like

$$I(a) = \int_0^\infty i(k)G(k,a)kdk \tag{1}$$

Introducing the Fourier transforms of functions i and G and making use of the Parseval's theorem, the integrated irradiance can be expressed as

$$I(a) \sim \int_0^\infty C(x)g(x,1/a)xdx, \tag{2}$$

where $g(x,1/a)$ denotes the Fourier transform of the filter function. We evaluated the integrated irradiance for several specific distribution of the far-field intensity and for a ring-like filter such as the one shown in Fig. 2 by using

$$\int_0^\infty C(x[k_2 J_1(x\frac{k_2}{a}) - k_1 J_1(x\frac{k_1}{a})]dx \tag{3}$$

In the case of a gaussian ACF $C(x) \sim \exp(-(x/L)^2)$ the integrated irradiance becomes

$$I(a) \sim [\exp(-\frac{k_1^2 L^2}{4a^2}) - \exp(\frac{k_2^2 L^2}{4a^2})]. \tag{4}$$

This function is plotted in Fig. 3 for several values of the surface autocorrelation length L.

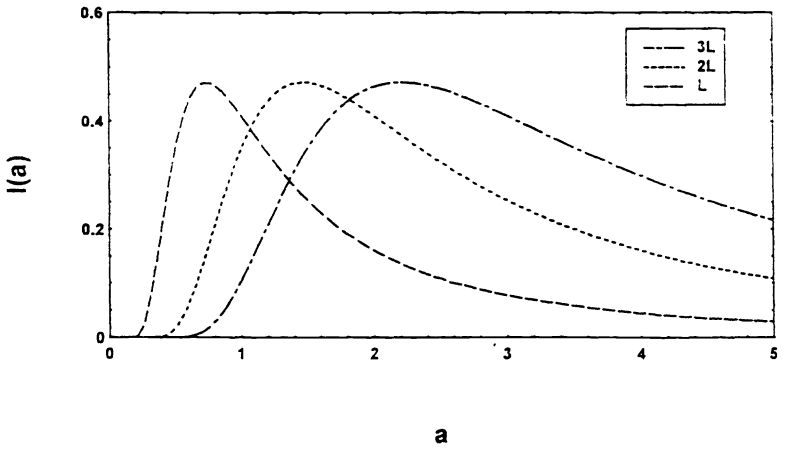

Fig.3 Integrated irradiances evaluated for $k_2/k_1 = 3/4$ and various autocorrelation lengths as indicated.

As can be seen, when plotted as a function of magnification parameter, the integrated irradiance has a maximum at a location

$$a^* = \frac{L}{2}\sqrt{\frac{k_2^2 - k_1^2}{2\ln(\frac{k_2}{k_1})}} \tag{5}$$

depending upon the value of the autocorrelation length and filter's parameters. Providing that the ACF and the filter shape are known, we can monitor the value of the surface autocorrelation length by making use of Eq. 5.

For negative exponential shape of the ACF $C(x) \sim \exp(-x/L)$, the corresponding integrated irradiance is given by

$$I(a) \sim \frac{1}{L}\left[\frac{1}{\sqrt{\frac{1}{L^2}+\frac{k_1^2}{a^2}}} - \frac{1}{\sqrt{\frac{1}{L^2}-\frac{k_2^2}{a^2}}}\right] \tag{6}$$

and the maximum is now located at

$$a^* = L\sqrt{\frac{k_2^2(\frac{k_1}{k_2})^{4/3} - k_1^2}{1-(\frac{k_1}{k_2})^{4/3}}}. \tag{7}$$

If similar evaluation is made for a more general shape of ACF, $C(x) \sim \exp(-(x/L)^\alpha)$ with $1 \leq \alpha \leq 2$, the resultant integrated irradiance is of the form of

$$I(a) \sim \frac{1}{\alpha}\sum_{m=0}^{\infty}\left\{\frac{(-1)^m\Gamma(\frac{2m+2}{\alpha})}{m!(m+1)!}\frac{L^{2m+2}k_1^{2m+2}}{a^{2m+2}}\left[(\frac{k_1}{k_2})^{2m+2}-1\right]\right\} \tag{8}$$

It should be pointed out that in a practical attempt to measure $I(a)$ with a setup such as the one in Fig.1, the maximum position can be adjusted in an optimum range of irradiance by modifying the focal length of the lens L or by changing the filter parameters. Based on measurements of integrated irradiance, we can infer characteristic lengths on the surface profile. However, the surface description is based on the *a priori* knowledge of surface ACF. If this is not known, the inverse scattering problem has to be solved. We will show next that the complete form of ACF can be retrieved from the values of $I(a)$ if the integrated irradiance is described in the frame of the integrated wavelet transformation.

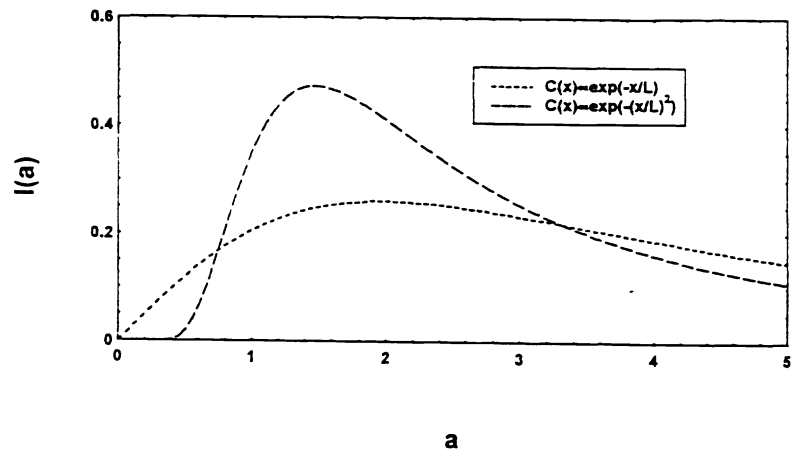

Fig.4 Integrated irradiances evaluated for $k_2/k_1 = 3/1$ and different autocorrelation functions of surface profile.

Integrated irradiances corresponding to different ACFs having similar autocorrelation lengths are presented in Fig. 4. The behavior of the integrated irradiance definitely depends on the shape of ACF suggesting that $I(a)$ can be used to infer the surface autocorrelation. This inversion procedure will be analyzed in the following sections.

IV. Integrated wavelet transform

The two-dimensional transformation of an input function $f(\mathbf{x})$ with respect to the wavelet $g(\mathbf{x})$ is defined as[7]

$$T_f(a,r,\mathbf{b}) = \frac{1}{a^2}\int g^*(\frac{r^{-1}(\mathbf{x}-\mathbf{b})}{a})f(\mathbf{x})d\mathbf{x} = \frac{1}{(2\pi)^2}\int G^*(ar^{-1}\mathbf{k})F(\mathbf{k})\exp(i\mathbf{bk})d\mathbf{k} \qquad (9)$$

where the symbol $*$ stands for complex conjugate and a, r, and $\mathbf{b}$ indicate the magnification, the rotation and the position in the wavelet domain, respectively. It should be noted that $T_f(a,r,\mathbf{b})$ and the product $G^*(ar^{-1}\mathbf{k})F(\mathbf{k})$ are Fourier-transform pair. In fact the second identity in Eq. 9 describes an operation of spatial filtering that is realized by a double diffraction imaging system with a standard 4F geometry. In this case the filter function is $G^*(ar^{-1}\mathbf{k})$. It worth noting that by doing the transformation of Eq. 9, no information about the input function $f(\mathbf{x})$ is lost as long as the wavelet admissibility condition, namely $\frac{1}{(2\pi)^2}\int\frac{|G(\mathbf{k})|^2}{\mathbf{k}^2}d\mathbf{k} < \infty$, is satisfied.

The irradiance in the wavelet transform plane can be integrated over the whole plane and an integrated wavelet transformation (IWT) is, accordingly, defined as

$$I(a,\theta) = \int \mid T_f(a,r,\mathbf{b}) \mid^2 d\mathbf{b} \qquad (10)$$

where θ is the angle that describes the wavelet rotation r. By using Parseval's theorem, the integral of Eq. 10 can be evaluated in the filter plane and it can be shown that[8]

$$I(a,\theta) = \frac{1}{a^2}\int C(\frac{r^{-1}x}{a})g(x)d(x) \qquad (11)$$

where, C and g are, as before, the autocorrelation functions of the input and wavelet function, respectively.

As we mentioned in Introduction, in the particular case of smooth surfaces there is a Fourier transform relationship between the ACF of surface fluctuations and the corresponding power spectrum. Therefore, the IWT transformation can be directly applied in the description of light scattering by smooth surfaces. If the admissibility condition is satisfied, Eq. 11 can be inverted and the surface ACF can be retrieved from the values of the integrated irradiance in the wavelet transform plane. This represents a new approach to the inverse problem associated to

scattering from slightly rough surfaces. The experimental data are not anymore the values of the angular-resolved scattered intensify but the values of the integrated irradiance as a function of filter magnification. We have studied the inverse problem in the particular case of the so-called Mexican-hat wavelet described in the Fourier plane by

$$G(k) = k^2 \exp(-\frac{k^2}{2}) \tag{12}$$

and in the case of Haar wavelet

$$H(k) = \frac{d}{2}[\frac{J_1(\pi dk)}{k} - \sqrt{2}\frac{J_1(\sqrt{2}\pi d\frac{k}{2})}{k}] \tag{13}$$

with d being a dilation parameter. These two wavelet function and their corresponding binary approximations are presented in Fig. 5.

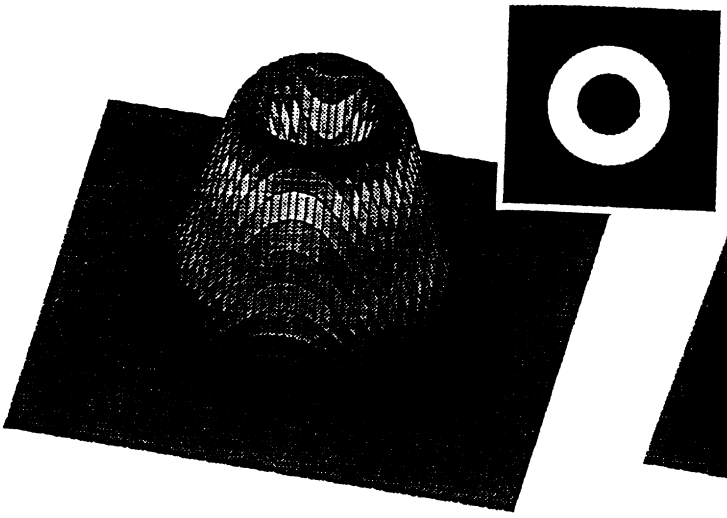

Fig.5a Mexican-hat wavelet described by Eq.12 and the corresponding binary approximation.

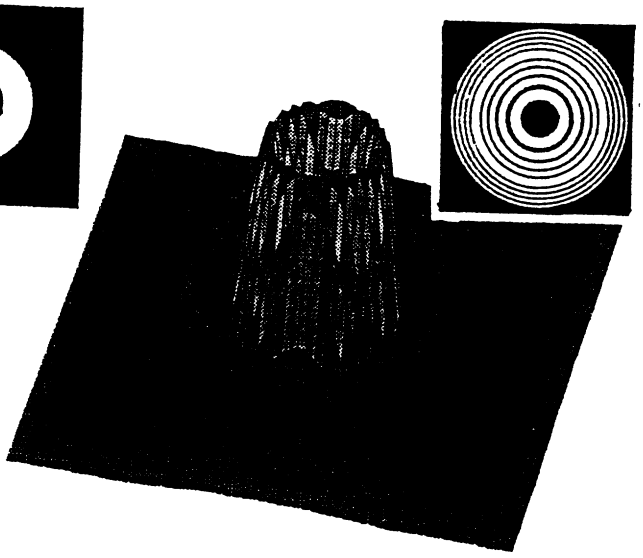

Fig.5b Haar wavelet described by Eq.13 and the corresponding binary approximation.

We selected these particular wavelet functions due to their relative simple optical implementation. In fact, the integrated irradiance function evaluated in Sect. II can be regarded as the integrated wavelet transformation corresponding to an approximate Mexican-hat such as the one in Fig. 5a.

V. Autocorrelation function retrieval

We generated power spectra corresponding to smooth surfaces with given ACF and we evaluated the integrated irradiance as a function of wavelet magnification. As the admissibility

condition is fulfilled for wavelet filters such as in Fig. 5, the Eq. 11 can be inverted to infer the ACF:

$$C(x) = \frac{1}{a^3} \int g(\frac{r^{-1}x}{a}) I(a,\theta) da d\theta. \tag{14}$$

The reconstruction formula of Eq. 14 was applied to integrated irradiances $I(a)$ corresponding to various surfaces having a gaussian shape of ACF. In Fig. 6 we present the reconstructed ACF obtained by using a Mexican hat with $h_2/h_1 = 3/1$ and corresponding to different autocorrelation lengths L . The autocorrelation length is successfully recovered as can be seen by simple inspection of the $1/e$ values of ACFs.

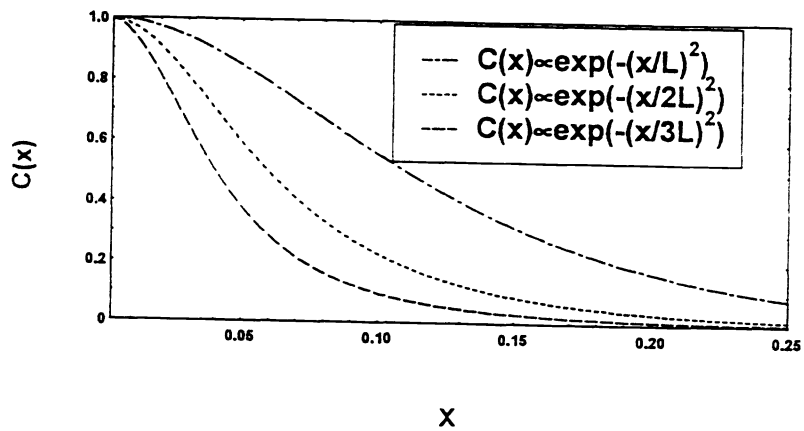

Fig.6 ACF reconstructed by IWT inversion technique. The curves correspond to Gaussian ACF with autocorrelation lengths as indicated.

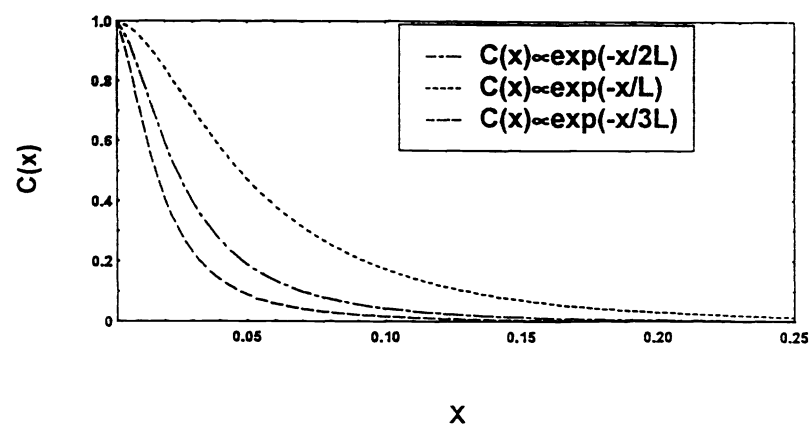

Fig.7 ACF reconstructed by IWT inversion technique. The curves correspond to negative exponential ACF with autocorrelation lengths as indicated.

The reconstruction procedure is insensible to the specific shape of ACF and, therefore, similar conclusions can be drawn for the case of negative exponential type of ACF proving that As expected, analogous results were obtained for reconstruction by using Haar wavelets. In practical optical implementation, however, the choice of a particular wavelet could be important because is dictated by sensitivity requirements of the detection system.

VI. Limited domain of magnifications

As we discuss in Introduction, the collection of scattering data is the main source of errors in an inversion procedure. In a practical experiment, one has access to a limited set of data, in our case to a limited range of the magnification parameter $a_{\min} < a < a_{\max}$. This limitation corresponds to the limited domain of angular scattering data collected in ARS technique. We studied the effect of narrowing the accessible interval of a on the reconstruction procedure. The principal remark is that the upper $a_{\max}$ and lower $a_{\min}$ limit of magnification domain have different effects on the shape of reconstructed ACF. A decrease in the value of $a_{\max}$ practically does not affect the recovered ACF as can be seen in Fig. 8b where a Gaussian function is retrieved by means of an inverse IWT using different intervals for a as indicated. On the other hand, when increasing $a_{\min}$ significant reconstruction errors are present especially at large correlation distances x. This is simply explained by an actual suppression of the low-scattering-angle contributions that, due to the Fourier transform relationship, determine the ACF attenuation at large distances x. This effects are to be carefully considered especially when reconstructing ACF with reduced autocorrelation lengths.

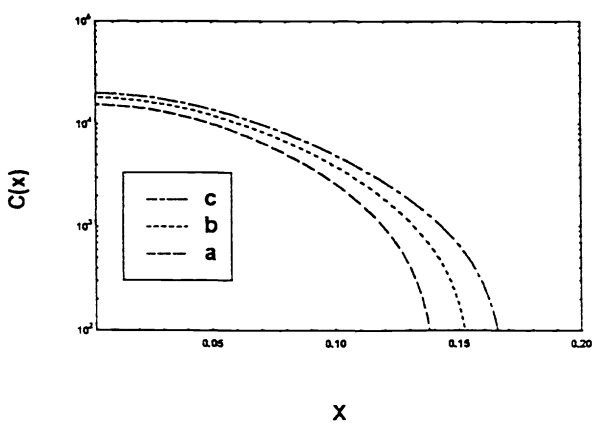

Fig. 8a Effect of increasing $a_{\min}$. Curves a,b,c correspond to $a_{\min}$=40,20,1, respectively, and $a_{\max}$=100.

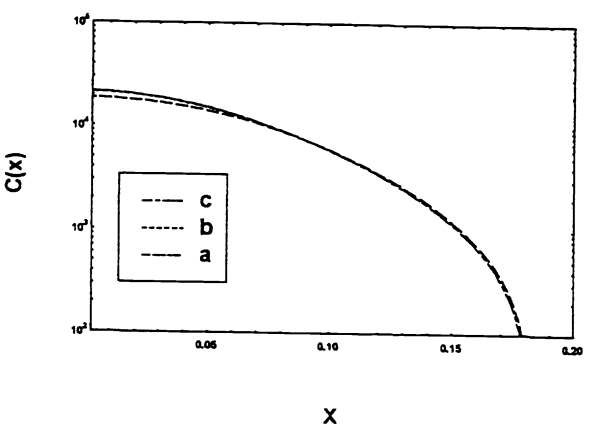

Fig. 8b Effect of increasing $a_{\max}$. Curves a,b,c correspond to $a_{\max}$=60,80,100, respectively, and $a_{\min}$=1.

A further reduction of the magnification interval results in unavoidable oscillations in the shape of the recovered ACF. In an experimental setup such as the one shown in Fig. 1, one can take advantage of an adjustable dilation of the power spectra and adjust the spatial extension of $I(k)$ to correspond to the appropriate domain of filter magnifications $[a_{\min}, a_{\max}]$.

VII. Noise influence

To simulate difficult experimental conditions, noise was added to the far-field intensity distribution. Typical example of scattered intensities are shown in Fig. 9a in the case of Gaussian

ACF. The corresponding ACF, retrieved by IWT, are presented in Fig. 9b. Also shown in Figs. 9a and 9b are $i(k)$ and, respectively, $C(x)$ corresponding to the case without additional noise.

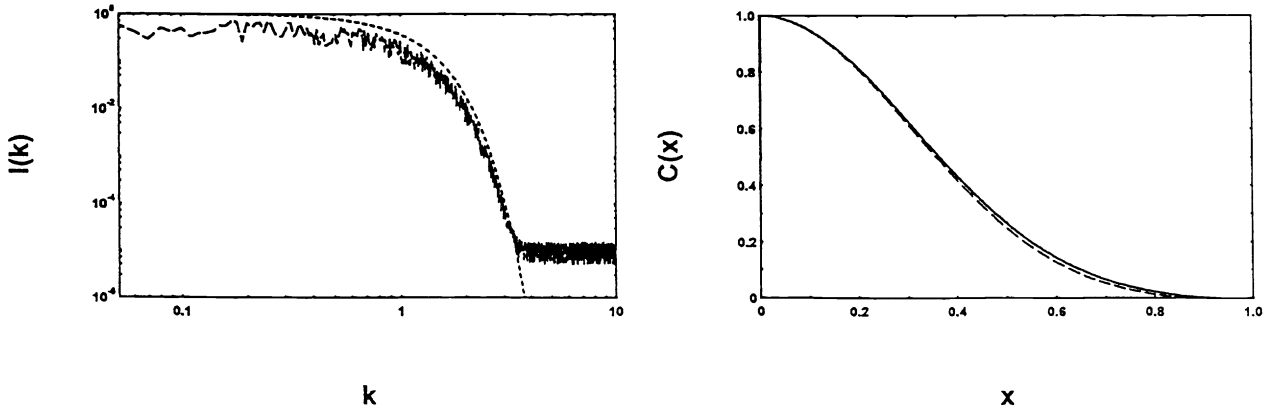

Fig.9 Reconstruction of a Gaussian ACF (b) form noisy data (a). The dashed curves in (a) and (b) correspond to the case without noise.

As can be seen, the effect of the speckle noise is almost suppressed in the behavior of ACF. This characteristic of IWT procedure can be understood as an effect of the use of a smooth monotonic function rather than a stepwise function to analyze the behavior of the scattered intensity.

VIII. Dynamic range

Another advantage of using the IWT procedure is a reduced dynamic range required for the detection system. To exemplify this we use the particular example of light scattering from fractal-like surfaces. It is well known that, in the case of fractal surfaces, the corresponding power spectrum has a power law dependence on the scattering angle.[9] To ensure the scaling behavior, the intensities span over many orders of magnitude as shown in Fig. 10a requiring a very large dynamic range of the detection system. To simulate practical conditions we used intensity data strongly corrupted by noise. However, we can integrate the angular-resolved intensity by using the IWT procedure. In Fig. 10b the integrated irradiance corresponding to a binary approximation for the Mexican hat having $h_2/h_1 = 3/1$ is presented. The reduced dynamic range is evident and, besides, the speckle noise is drastically diminished. Using data in Fig. 10b, inverse IWT were processed and the results are presented in Fig. 10c together with the expected dependencies for the ACFs. As can be seen, the power-law behaviors are fully recovered in spite of the noisy intensities and a dynamic range of only 50 for the magnification parameter a. Note that a ACF retrieval by using an inverse Fourier transformation of the intensity data in Fig. 10a would require a dynamic range of almost five times larger than IWT.

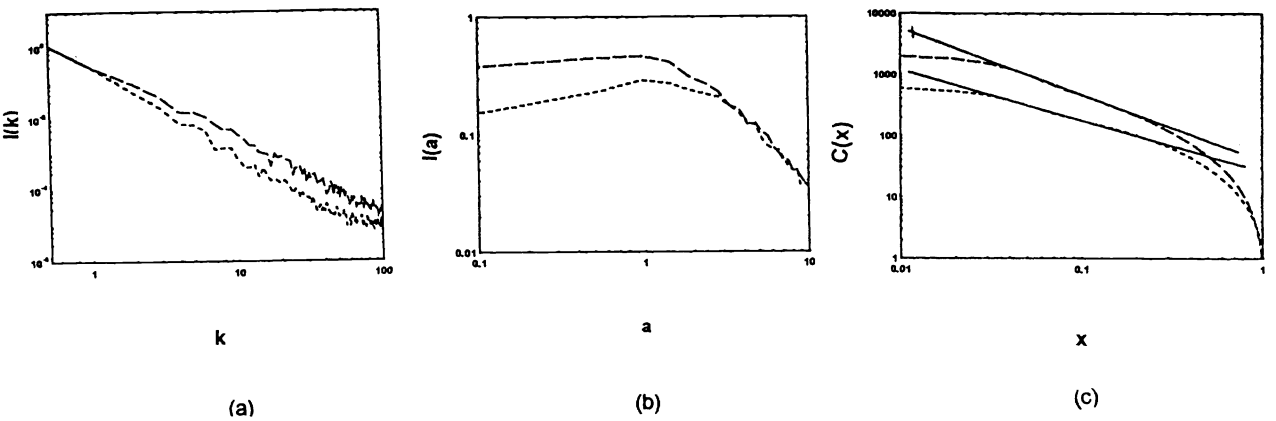

Fig.10 Reconstruction of power-law ACF corresponding scaling exponents of 2 and 2.5: (a) angular-resolved intensities, (b) integrated irradiances, and (c) the retrieved ACF. The straight lines in (c) are the expected dependencies.

IX. Conclusions

The random aspects of a rough surface are described by the ACF of the surface profile and the height distribution. In certain cases, the surface characteristics can be derived from the scattered intensity as a function of angle. For smooth surfaces, the Fourier transform of the diffuse component of the scattered radiation yields the ACF. We described the diffuse component in terms of an integral wavelet transform of the surface height variations. The inversion procedure uses the values of the far-field integrated irradiance as a function of the magnification of the measuring aperture (wavelet filter). We presented the inversion technique and showed that the retrieval procedure is insensible to the specific shape of the ACF. The effects of reducing the magnification interval were also studied. As experimental values of the scattered intensities are usually corrupted by speckles, we analyzed the inversion procedure in these conditions and we proved that the noise effects are practically suppressed in the IWT. The basic advantage of this formalism is the use of a smooth monotonic function rather than a stepwise function for the analyzing aperture. Another characteristic that is appealing for practical implementations of the measurement is a reduced dynamic range required for the detection system as compared to the inverse Fourier transformation of the angular-resolved scattered intensities.

References

[1]E. Marx, B. Leridon, T. R. Lettieri, J,-F. Song, and T. V. Vorburger, "Autocorrelation functions from optical scattering for one-dimensionally rough surfaces", *Appl. Opt.* 32, 67-76, 1993.

[2]J. A. Ogilvy, *Theory of wave scattering from random surfaces*, Adam Hilger, Bristol, 1991.

[3]P. J. Chandley, "Determination of the autocorrelation function of height on a rough surface from coherent light scattering", *Opt. Quant. Electr.* 8, 329-333, 1976.

[4]E. Marx and T. Vorburger, "Direct and inverse problems for the light scattered by rough surfaces", *Appl. Opt.* 29, 3613-3626, 1990.

[5]J. M. Bennett and L. Mattson, *Introduction to surface roughness and scattering*, Optical Society of America, Washington, D. C., 1989.

[6]A. Dogariu, J. Uozumi, and T. Asakura, "Determination of surface roughness parameters using the integrated intensity", *Optik* 93, 52-58, 1993.

[7]A. Grossmann and J. Morlet, "Decompositions of functions into wavelets of constant shape, and related transforms", in *Mathematics and physics, lectures on recent results*, ed. L. Streit, World Scientific, Singapore, 1985.

[8]A. Dogariu, J. Uozumi, and T. Asakura, "Wavelet transform analysis of slightly rough surfaces", *Opt. Commun.* 107, 1-5, 1994.

[9]E. L. Church, "Fractal surface finish", *Appl. Opt.* 8, 1518-1526, 1988.